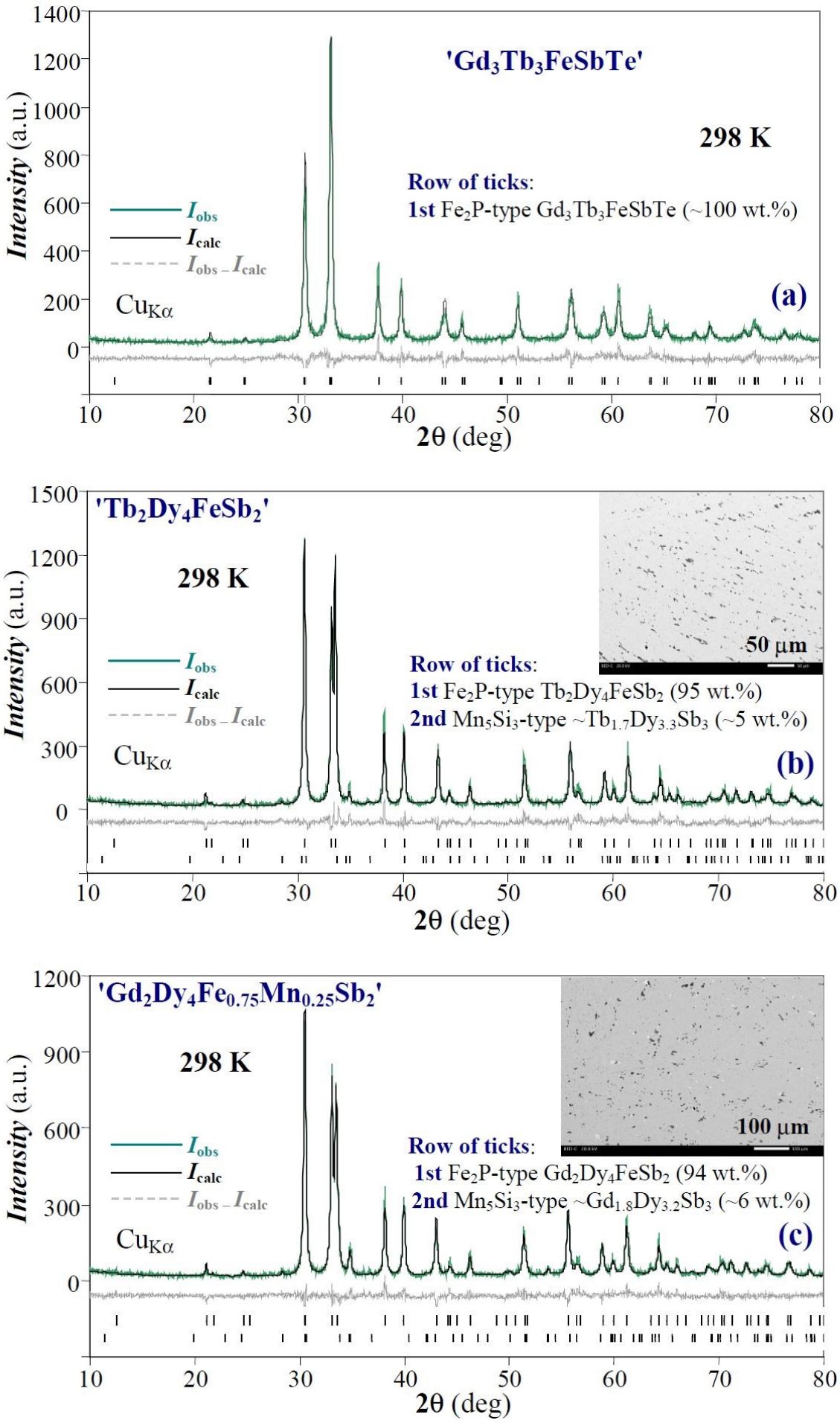

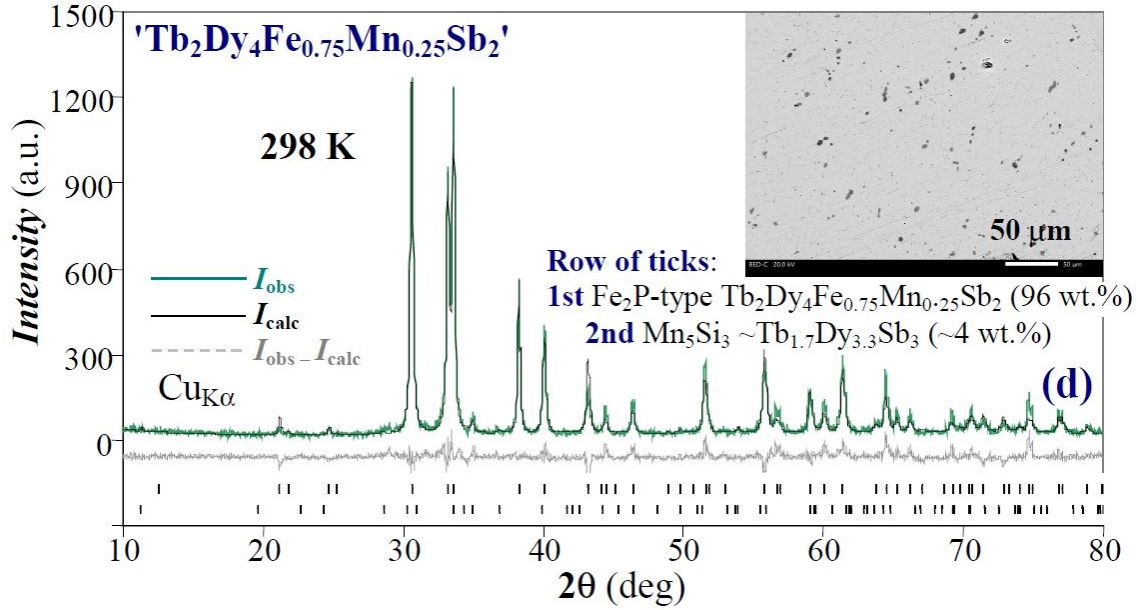
'Tb2Dy4Fe0.75Mn0.25Sb2'
298 K
50 μm
Row of ticks:
1st Fe2P-type Tb2Dy4Fe0.75Mn0.25Sb2 (96 wt.%)
2nd Mn5Si3 ~Tb1.7Dy3.3Sb3 (~4 wt.%)
Iobs
Icalc
Iobs – Icalc
CuKα
(d)
Intensity (a.u.)
2θ (deg)

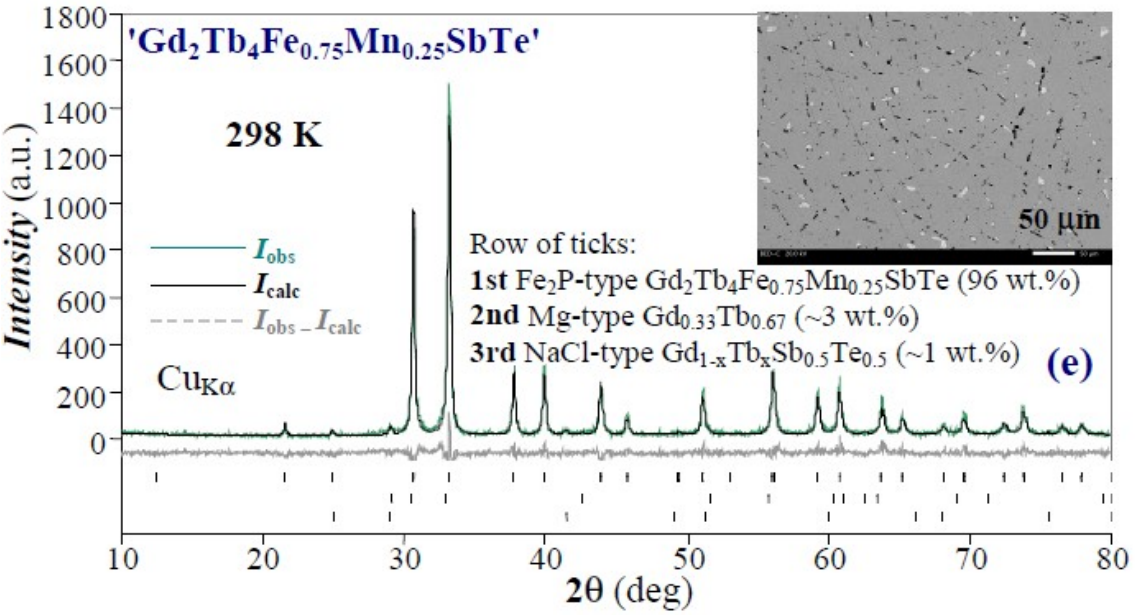
'Gd2Tb4Fe0.75Mn0.25SbTe'
298 K
50 μm
Row of ticks:
1st Fe2P-type Gd2Tb4Fe0.75Mn0.25SbTe (96 wt.%)
2nd Mg-type Gd0.33Tb0.67 (~3 wt.%)
3rd NaCl-type Gd1-xTbxSb0.5Te0.5 (~1 wt.%)
Iobs
Icalc
Iobs – Icalc
CuKα
(e)
Intensity (a.u.)
2θ (deg)

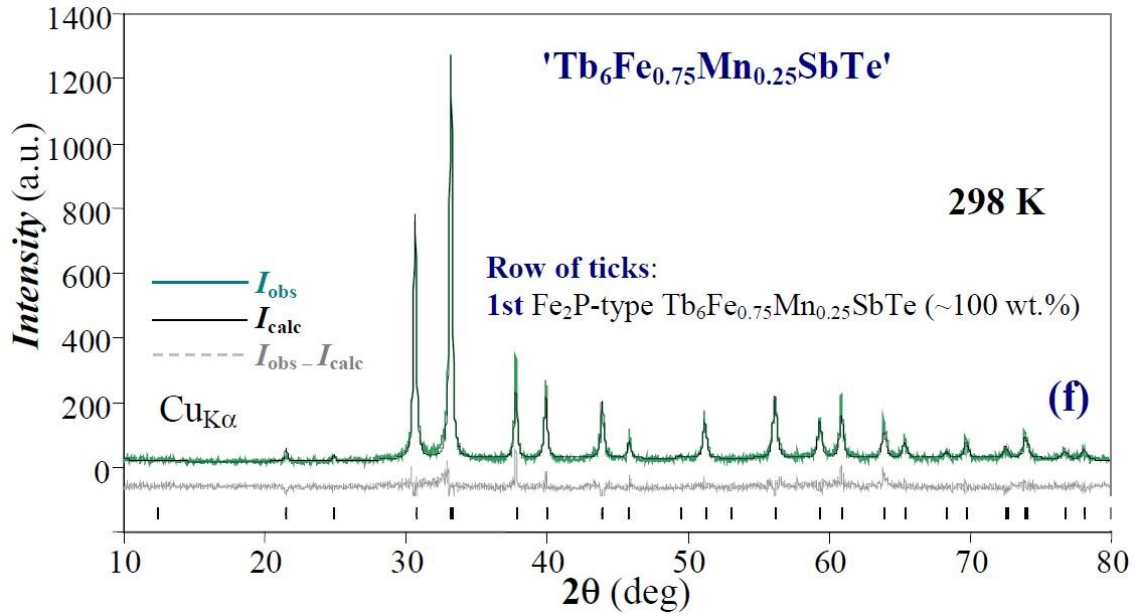
'Tb6Fe0.75Mn0.25SbTe'
298 K
Row of ticks:
1st Fe2P-type Tb6Fe0.75Mn0.25SbTe (~100 wt.%)
Iobs
Icalc
Iobs – Icalc
CuKα
(f)
Intensity (a.u.)
2θ (deg)

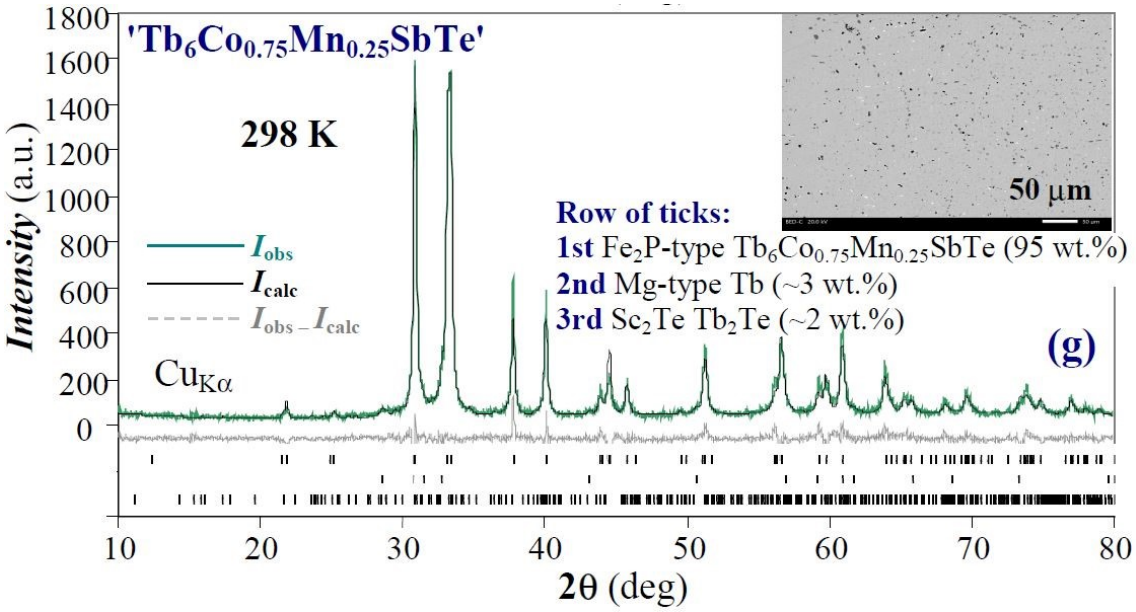
'Tb6Co0.75Mn0.25SbTe'
298 K
50 μm
Row of ticks:
1st Fe2P-type Tb6Co0.75Mn0.25SbTe (95 wt.%)
2nd Mg-type Tb (~3 wt.%)
3rd Sc2Te Tb2Te (~2 wt.%)
Iobs
Icalc
Iobs – Icalc
CuKα
(g)
Intensity (a.u.)
2θ (deg)

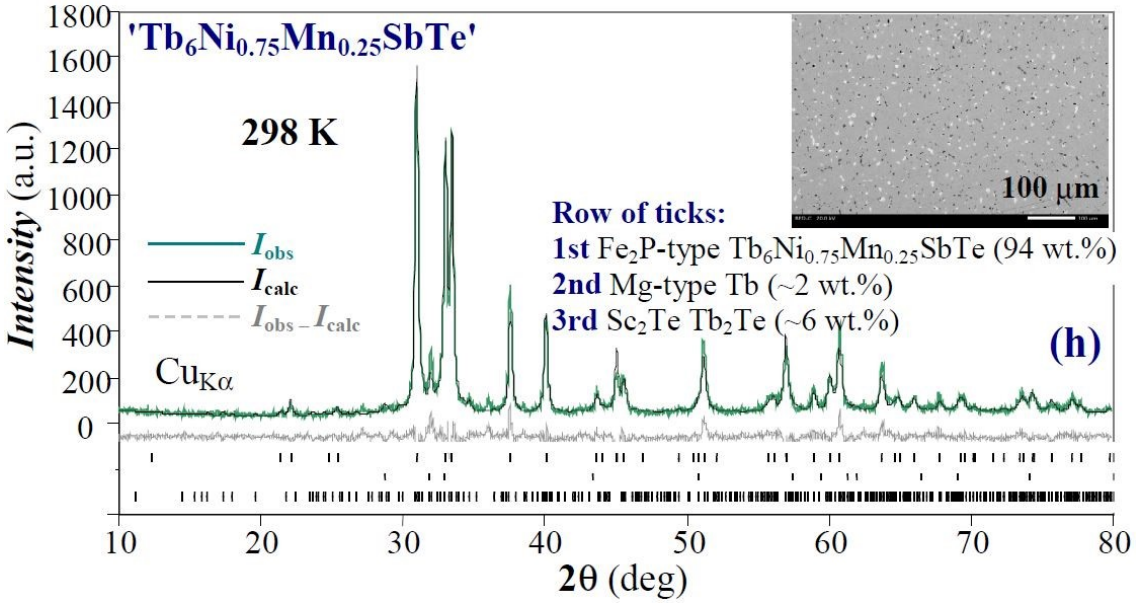
'Tb6Ni0.75Mn0.25SbTe'
298 K
100 μm
Row of ticks:
1st Fe2P-type Tb6Ni0.75Mn0.25SbTe (94 wt.%)
2nd Mg-type Tb (~2 wt.%)
3rd Sc2Te Tb2Te (~6 wt.%)
Iobs
Icalc
Iobs – Icalc
CuKα
(h)
Intensity (a.u.)
2θ (deg)

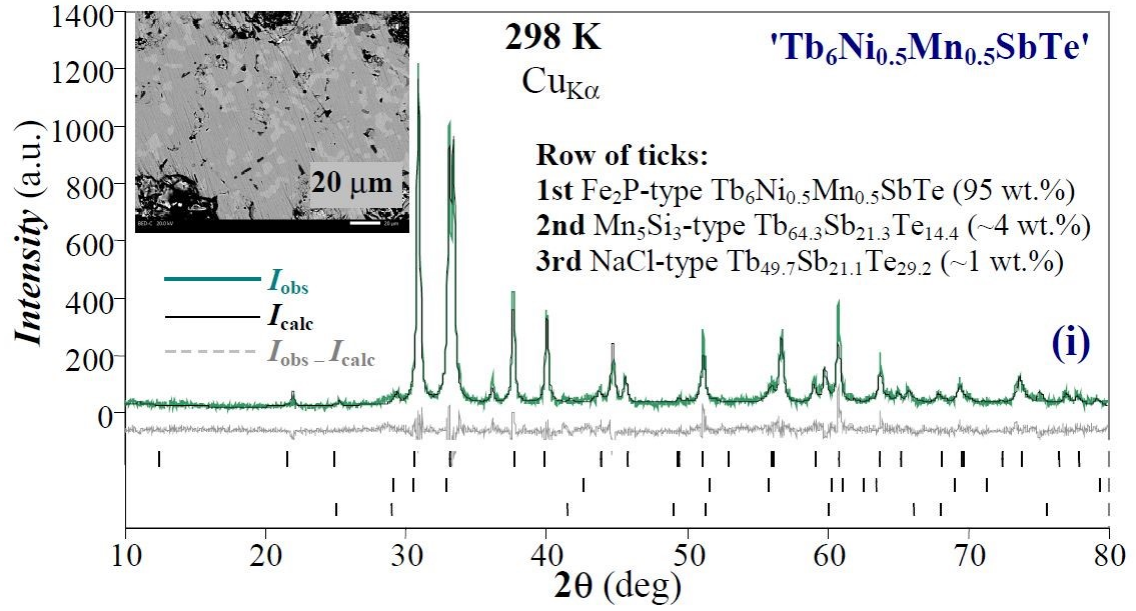
'Tb6Ni0.5Mn0.5SbTe'
298 K
CuKα
20 μm
Row of ticks:
1st Fe2P-type Tb6Ni0.5Mn0.5SbTe (95 wt.%)
2nd Mn5Si3-type Tb64.3Sb21.3Te14.4 (~4 wt.%)
3rd NaCl-type Tb49.7Sb21.1Te29.2 (~1 wt.%)
Iobs
Icalc
Iobs – Icalc
(i)
Intensity (a.u.)
2θ (deg)

Figure 1s. Rietveld refinement of X-ray powder diffraction patterns of **(a)** 'Gd$_3$Tb$_3$FeSbTe', **(b)**'Tb$_2$Dy$_4$FeSb$_2$', **(c)** 'Gd$_2$Dy$_4$Fe$_{0.75}$Mn$_{0.25}$Sb$_2$', **(d)** 'Tb$_2$Dy$_4$Fe$_{0.75}$Mn$_{0.25}$Sb$_2$', **(e)** 'Gd$_2$Tb$_4$Fe$_{0.75}$Mn$_{0.25}$SbTe', **(f)** 'Tb$_6$Fe$_{0.75}$Mn$_{0.25}$SbTe', **(g)** 'Tb$_6$Co$_{0.75}$Mn$_{0.25}$SbTe', **(h)** 'Tb$_6$Ni$_{0.75}$Mn$_{0.25}$SbTe' and **(i)** 'Tb$_6$Ni$_{0.5}$Mn$_{0.5}$SbTe'. Inset in **Figures b**, **c**, **d**, **e**, **g**, **h** and **i**: microstructure of sample. The references of ticks are marked and compositions of alloys are given in **Figures**.

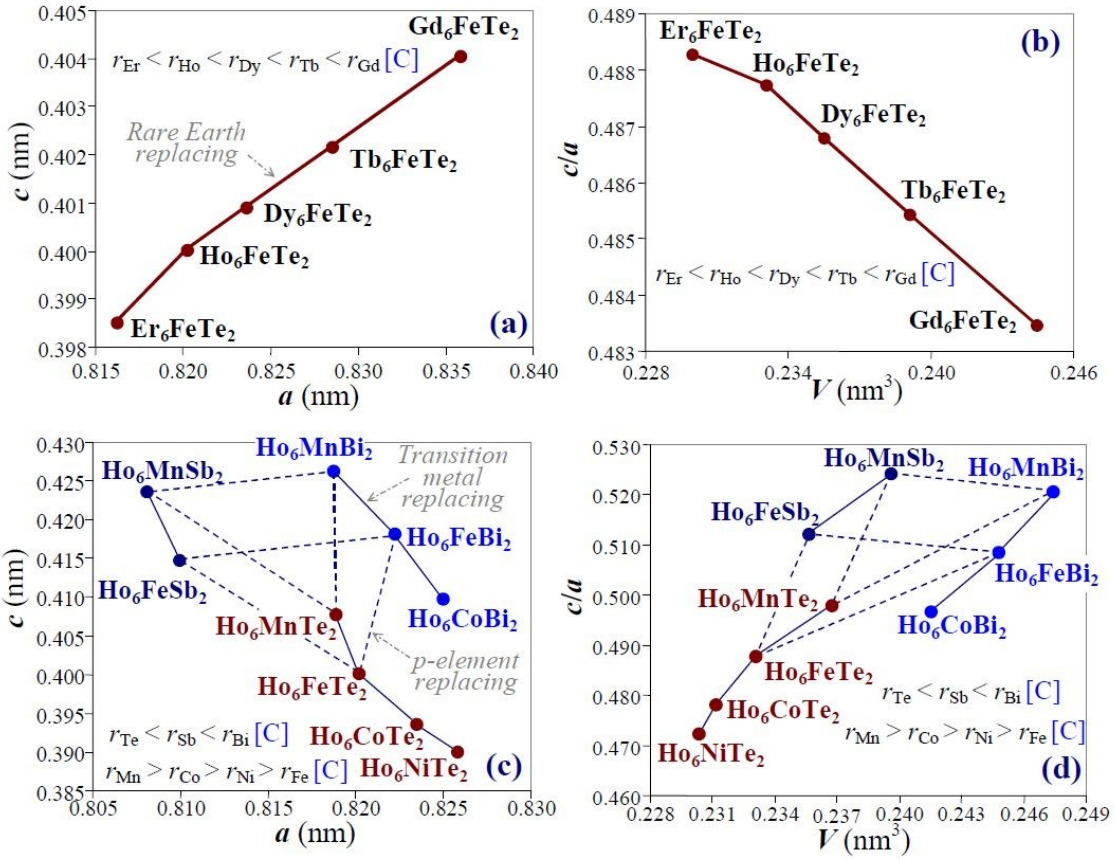

Figure 2s. Unit cell data of ternary Fe$_2$P-type {Gd-Er}$_6$FeTe$_2$ tellurides: **(a)** cell parameter *c* vs cell parameter *a* and **(b)** *c*/*a* ratio vs unit cell volume *V* (replacing of rare earth leads to monotonic increasing of *a* and *c* cell parameters and unit cell volume *V* with slight decreasing of *c*/*a* ratio from Gd$_6$FeTe$_2$ to Er$_6$FeTe$_2$) and unit cell data of Ho-based Ho$_6${Fe, Mn}Sb$_2$ antimonides, Ho$_6${Mn-Ni}Te$_2$ tellurides and Ho$_6${Mn, Fe, Co}Bi$_2$ bismuthides: **(c)** cell parameter *c* vs cell parameter *a* and **(d)** *c*/*a* ratio vs unit cell volume *V*. Despite the increasing of atomic radii from Fe to Mn and from Te to Bi (the sequence of atomic radii is given in **Figures**), the replacing of transition metals leads to increasing of *a* cell parameter and decreasing of *c* cell parameter, unit cell volume *V* and *c*/*a* ratio in the 'Mn-Fe-Co-Ni' row. The replacing of Sb for Bi leads to expansion of unit cell in *ab*-plane and its slight expansion along *c* axis with increasing of unit cell volume *V* and decreasing of *c*/*a* ratio, while replacing of Sb for Te corresponds to the expansion of unit cell in *ab*-plane and its compression along *c* axis with decreasing of unit cell volume *V* and *c*/*a* ratio. The areas of possible transformation of unit cell of the Ho$_6$Fe$_{1-x}$Mn$_x$Sb$_{2-y-z}$Te$_y$Bi$_z$ quasiternary solid solution are shown in **Figures c** and **d**.

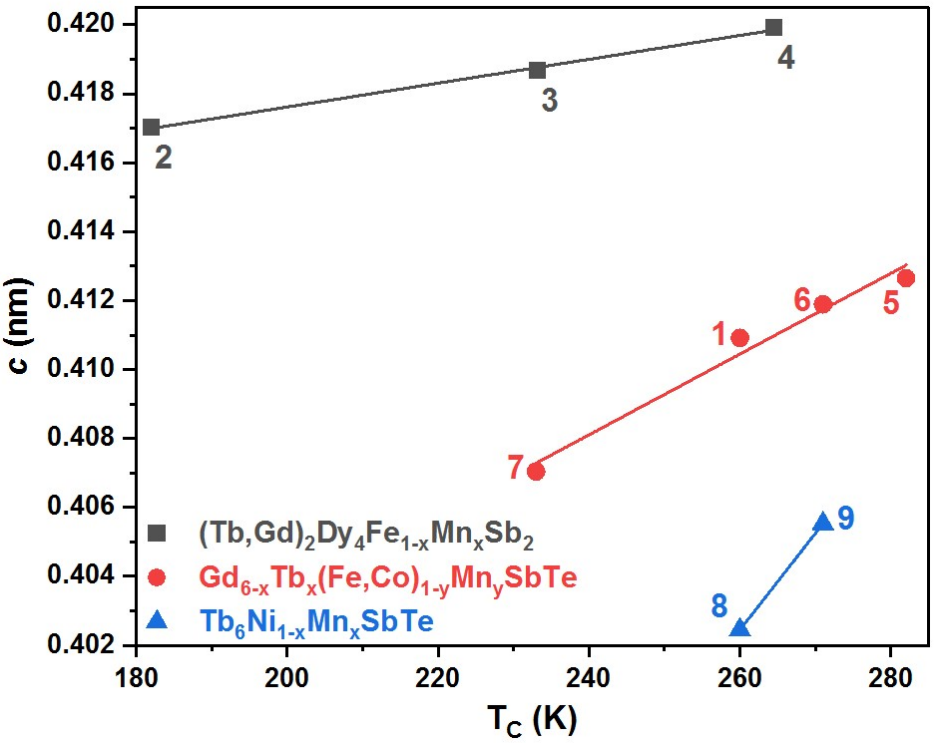

Figure 3s. General trends of T_C temperature with c cell parameter in $(Tb,Gd)_2Dy_4Fe_{1-x}Mn_xSb_2$ (grey), $Gd_{6-x}Tb_x(Fe,Co)_{1-y}Mn_ySbTe$ (red) and $Tb_6Ni_{1-x}Mn_xSbTe$ (blue) sub-families. Number labels are the ones used in Tables 1, 2, 3, 4 and Table 1s.

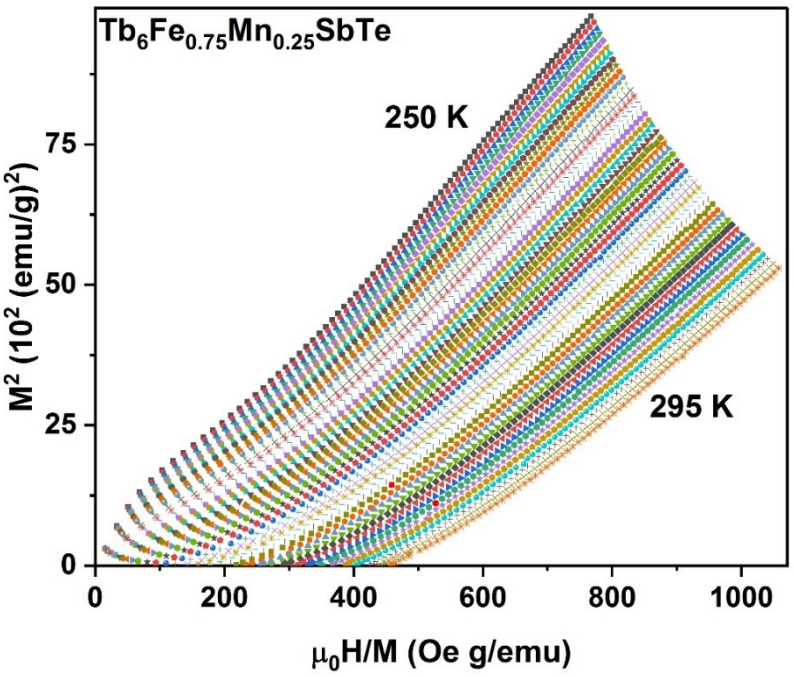

Figure 4s. Arrot Plot representation of magnetization isotherms around T_C for $Tb_6Fe_{0.75}Mn_{0.25}SbTe$. Positive slopes are indicative of the second order nature of this transition.

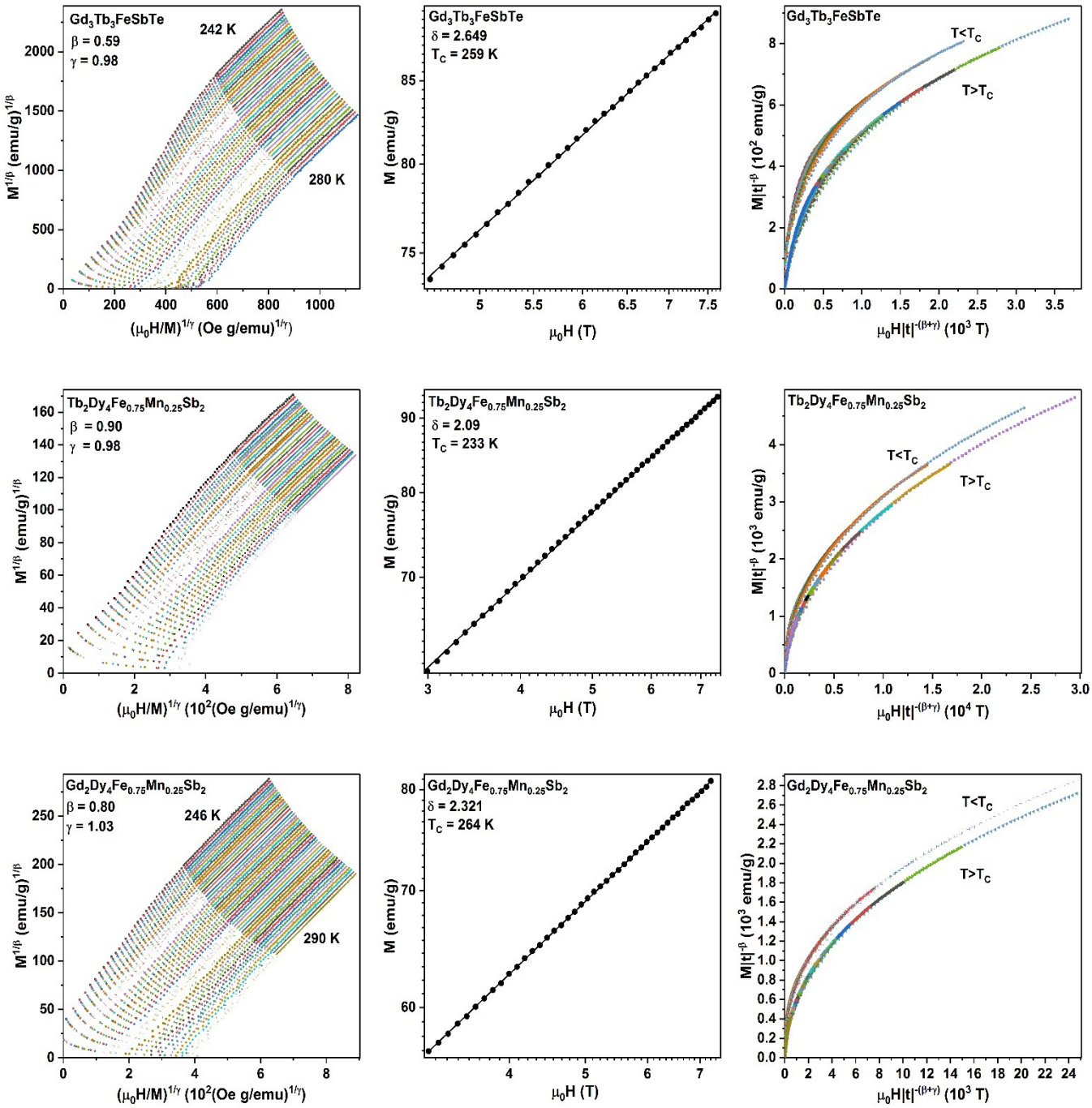

Figure 5s. From left to right: Optimized Modified Arrot Plot, M vs. $\mu_0 H$ plot in logarithmic scale for the critical isotherm and representation of the magnetic equation of state for $Gd_3Tb_3FeSbTe$ (top row), $Tb_2Dy_4Fe_{0.75}Mn_{0.25}Sb_2$ (middle row) and $Gd_2Dy_4Fe_{0.75}Mn_{0.25}Sb_2$ (bottom row).

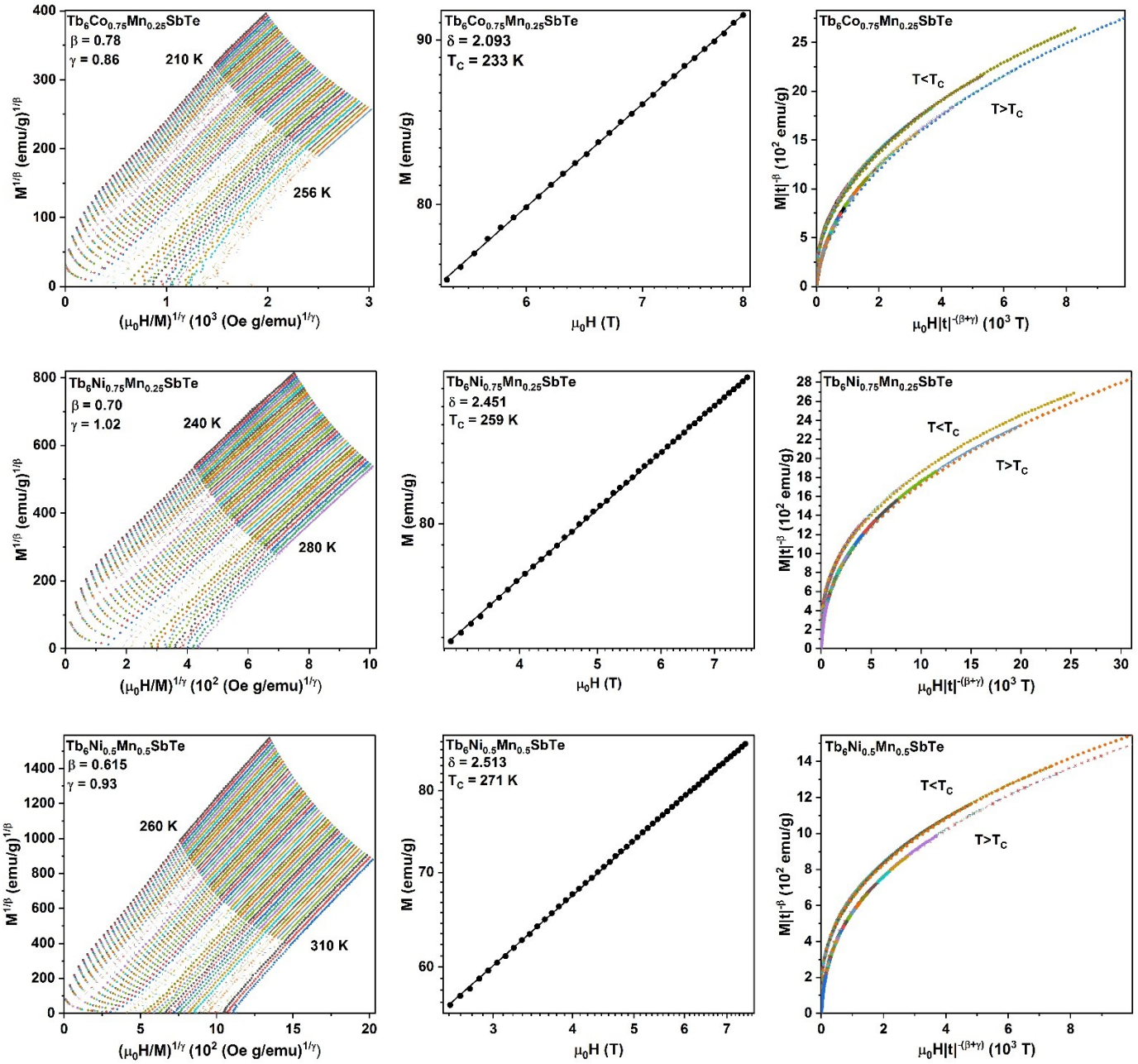

Figure 6s. From left to right: Optimized Modified Arrot Plot, M vs. $\mu_0 H$ plot in logarithmic scale for the critical isotherm and representation of the magnetic equation of state for $Tb_6Co_{0.75}Mn_{0.25}SbTe$ (top row), $Tb_6Ni_{0.75}Mn_{0.25}SbTe$ (middle row) and $Tb_6Ni_{0.5}Mn_{0.5}SbTe$ (bottom row).

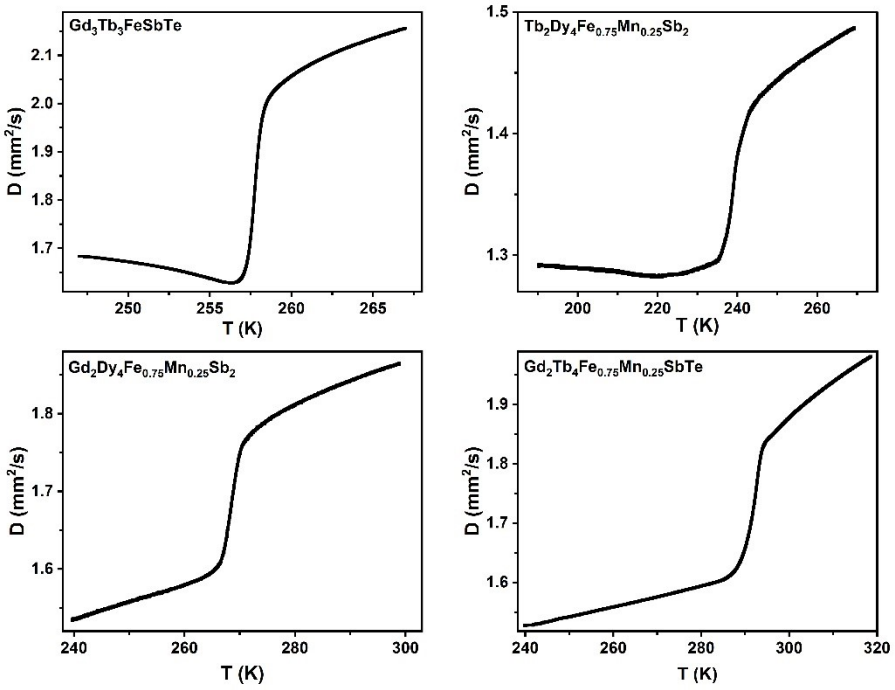

Figure 7s. Thermal diffusivity (D) as a function of temperature around T_C for $Gd_3Tb_3FeSbTe$, $Tb_2Dy_4Fe_{0.75}Mn_{0.25}Sb_2$, $Gd_2Dy_4Fe_{0.75}Mn_{0.25}Sb_2$ and $Gd_2Tb_4Fe_{0.75}Mn_{0.25}SbTe$.

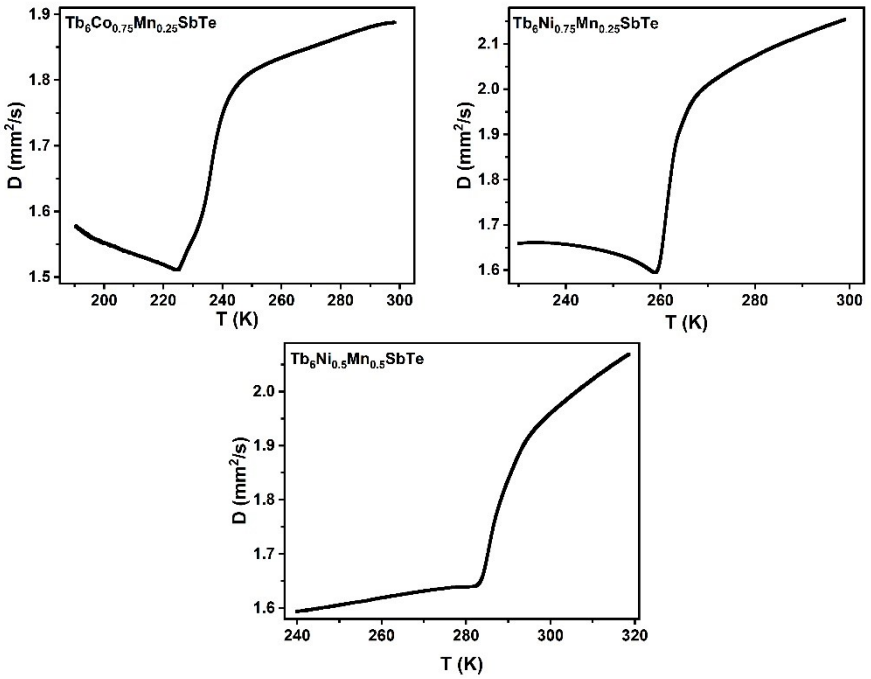

Figure 8s. Thermal diffusivity (D) as a function of temperature around T_C for $Tb_6Co_{0.75}Mn_{0.25}SbTe$, $Tb_6Ni_{0.75}Mn_{0.25}SbTe$ and $Tb_6Ni_{0.5}Mn_{0.5}SbTe$.

Table 1s. Alloy's content and unit cell data of phases.

N	Alloy	Phase	wt.%	Type	*a* (nm)	*b* (nm)	*c* (nm)	R_F (%)
1	'$Gd_3Tb_3FeSbTe$'	$Gd_3Tb_3FeSbTe$ [a-]	~100	Fe_2P	0.82712(2)		0.41051(1)	3.6
2	'$Tb_2Dy_4FeSb_2$'	$Tb_2Dy_4FeSb_2$	~95	Fe_2P	0.81481(5)		0.41703(2)	4.0
		~$Tb_{1.7}Dy_{3.3}Sb_3$	~5	Mn_5Si_3	0.8979(6)		0.6230(3)	5.8
3	'$Gd_2Dy_4Fe_{0.75}Mn_{0.25}Sb_2$'	$Gd_2Dy_4Fe_{0.75}Mn_{0.25}Sb_2$	~94	Fe_2P	0.81646(6)		0.41991(3)	4.2
		~$Gd_{1.8}Dy_{3.2}Sb_3$	~6	Mn_5Si_3	0.8937(4)		0.6289(3)	6.2
		~$Gd_{0.34}Dy_{0.66}$ [b-]	< 1	Mg				
4	'$Tb_2Dy_4Fe_{0.75}Mn_{0.25}Sb_2$'	$Tb_2Dy_4Fe_{0.75}Mn_{0.25}Sb_2$	~96	Fe_2P	0.81478(6)		0.41866(3)	4.8
		~$Tb_{1.7}Dy_{3.3}Sb_3$	~4	Mn_5Si_3	0.8990(9)		0.6251(4)	4.6
5	'$Gd_2Tb_4Fe_{0.75}Mn_{0.25}SbTe$'	$Gd_2Tb_4Mn_{0.25}Fe_{0.75}SbTe$	~96	Fe_2P	0.82577(5)		0.41265(3)	5.6
		$Gd_{0.33}Tb_{0.67}$	~3	Mg	0.35421(9)		0.5871(2)	4.3
		$Gd_{1-x}Tb_xSb_{0.5}Te_{0.5}$	~1	NaCl	0.6159(3)			3.9
		$Gd_{20.8}Tb_{46.6}Sb_{0.3}Te_{32.3}$ [b-]	<1	Sc_2Te				
6	'$Tb_6Fe_{0.75}Mn_{0.25}SbTe$'	$Tb_6Fe_{0.75}Mn_{0.25}SbTe$ [a-]	~100	Fe_2P	0.82337(3)		0.41179(1)	4.2
7	' $Tb_6Co_{0.75}Mn_{0.25}SbTe$'	$Tb_6Co_{0.75}Mn_{0.25}SbTe$	~95	Fe_2P	0.82547(6)		0.40704(2)	3.7
		Tb	~3	Mg	0.3607(2)		0.5650(3)	3.1
		Tb_2Te	~2	Sc_2Te	2.1988(13)	0.3965(2)	1.1536(6)	4.2
8	'$Tb_6Ni_{0.75}Mn_{0.25}SbTe$'	$Tb_6Ni_{0.75}Mn_{0.25}SbTe$	~94	Fe_2P	0.82927(7)		0.40245(3)	3.9
		Tb	~2	Mg	0.3597(2)		0.5612(4)	3.4
		Tb_2Te	~4	Sc_2Te	2.1815(12)	0.3971(2)	1.1578(4)	3.7
9	'$Tb_6Ni_{0.5}Mn_{0.5}SbTe$'	$Tb_6Ni_{0.5}Mn_{0.5}SbTe$	~95	Fe_2P	0.82840(7)		0.40553(3)	5.4
		$Tb_{64.3}Sb_{21.3}Te_{14.4}$	~4	Mn_5Si_3	0.9292(8)		0.5892(3)	6.6
		$Tb_{49.7}Sb_{21.1}Te_{29.2}$	~1	NaCl	0.6135(8)			4.0

[a-] Crystallographic data used with permission of JCPDS - International Centre for Diffraction Data (USA), [b-] from EDS analysis, only.

Table 2s. Theoretical magnetic critical exponents for several universality models. d dimensionality of the interaction, N number of spin components, β of spontaneous magnetization, γ of isothermal susceptibility, δ of critical isotherm [48-50, 52-57].

Universality class	d	N	β	γ	δ
Mean-field			0.5	1.0	3.0
2D-Ising	2	1	0.125	1.75	14
3D-Ising	3	1	0.3265	1.237	4.79
3D-XY	3	2	0.348	1.317	4.78
3D-Heisenberg	3	3	0.369	1.396	4.78
Chiral XY	3	2	0.253	1.13	5.47
Chiral-Heisenberg	3	3	0.30	1.17	4.90
Tricritical Mean Field			0.25	1.0	5.00
2D-Long range	2	1	0.298	1.393	5.67
3D-Ising spin glass	3	1	0.5	2.9	6.80